Volatile Organic Compound Detection Using Insect Odorant-Receptor Functionalised Field-Effect Transistors

by

Eddyn Oswald Perkins Treacher

A thesis submitted in fulfilment of the
requirements of the degree of
Doctor of Philosophy in Physics
School of Physical and Chemical Sciences
Te Herenga Waka - Victoria University of Wellington

May 2024

Table of contents

Acknowledgements

1. Carbon Nanotube and Graphene Field-Effect Transistors

1.1. Introduction

Out of a wide range of available transducer options available for the creation of compact, portable and highly-integrated biosensors, field-effect transistors are among the most promising. Field-effect transistors, initially proposed in the 1930s, consist of two conductive electrodes on either side of a semiconducting channel, the 'source' and 'drain' electrodes, alongside an isolated 'gate' electrode which is typically perpendicular to the channel. An applied electric field from the gate electrode capacitively controls channel resistance, giving rise to the label 'field-effect'. By adjusting gate voltage, the flow of charge carriers between source and drain can be varied over several orders of magnitude. The ability of this simple structure to obtain a large signal response from small changes in channel behaviour means field-effect transistors can be used as high-quality amplifiers for sensor applications [1]–[4].

Carbon nanotube network and graphene field-effect transistors (CNTFETs and GFETs) are both examples of a class of field-effect transistors called thin-film transistors (TFTs). These transistors, first developed in 1962 [5], are closely related to the commonly-used metal oxide semiconductor field-effect transistor (MOSFET). Unlike MOSFETs, thin-film transistors do not use the substrate as the device channel. Instead, current passes through a semiconducting film on the surface of the device; the films discussed here are graphene and carbon nanotubes, two carbon-based low-dimension nanomaterials. Since thin-film transistors do not require a conductive substrate, they can be fabricated using light, flexible and stretchable substrates, making them significantly more versatile than MOSFETs [1], [3], [6]. Invisible conductive thin-films such as metal oxides and carbon nanotube networks can also be used to create transparent electronics [6]. While the principle of modulating current with a gate electrode is shared by the MOSFET and TFT, the underlying physics behind the transistor behaviour differs between the two. The MOSFET is turned on by the change in carrier behaviour when switching from an depletion to an inversion mode, while this is not the case for a TFT [1]. Details of graphene and carbon nanotube TFT switching behaviours can be found in the subsequent sections.

1.2. Thin-Film Field-Effect Transistors

1.2.1. Structure and Gating

The basic components of the thin-film transistor can be configured in a number of different ways. Two of these configurations are the back-gated field-effect transistor and the liquid-gated (or electrolyte-gated) transistor. The relatively simple back-gated configuration, shown in Figure 1.1 (a), uses the degenerately doped silicon substrate as the gate. The channel is isolated from the gate with a thin silicon dioxide layer. A liquid-gated device, shown in Figure 1.1 (b), is used for sensitive analyte detection in liquid-phase. In the most common form of this configuration, a submerged Ag/AgCl reference electrode is used as a top-gate. The channel is isolated from the gate by the bulk of an electrolyte solution, typically the biofriendly phosphate-buffered saline (PBS). Other aqueous salt solutions, polymers and ion-gels are also sometimes used as the electrolyte gate. The electrolyte is restricted to the channel area using a hydrophobic PDMS microchamber, referred to here as a 'PDMS well' [2], [3], [7], [8].
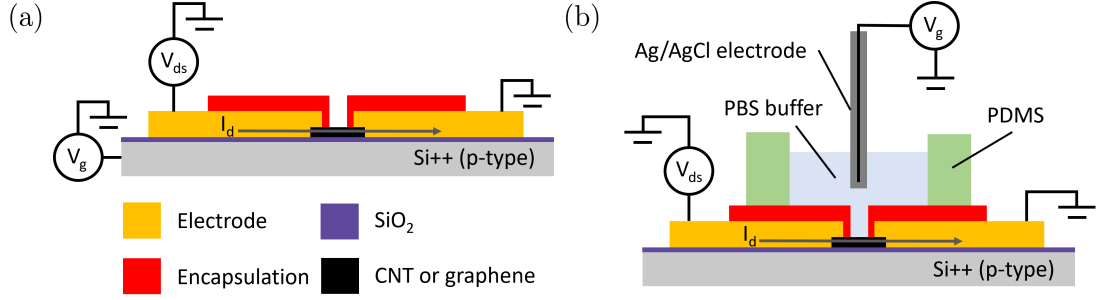

Figure 1.1.: Schematics (not to scale) showing the side-view cross-section of a thin-film field-effect transistor in both the (a) back-gated and (b) liquid-gated configuration. A graphene monolayer or a carbon nanotube network is used as the transistor thin-film. The drain electrode is the gold contact on the left side of each figure, while the source electrode is the gold contact on the right.

Two different voltages are used to adjust transistor operation. The first is the 'drain bias', V_{ds}, between the drain and source electrodes, and the second is the 'gate bias', V_g, applied between the gate and source electrode. The value of V_g determines how charge carriers flow under the influence of V_{ds} to produce a drain-source current I_d. The relative effect of changes in V_g on source-drain current I_d is determined by gate capacitance. In the general case, gate capacitance is a series combination of geometric capacitance, C_G, and the quantum capacitance of the channel nanomaterial, C_Q [2], [6]–[9]. Diameter and separation of nanotubes also play a role in the case of carbon nanotube networks [10]. In an ambipolar transistor, a highly negative V_g will give rise to hole conduction, and a highly positive V_g will give rise to electron conduction[4], [7], [8]. When $|V_{ds}| < |V_g| - |V_t|$ and the device is gated on, the device is in the linear regime. In this regime, V_{ds} is directly proportional to I_d, similar to an Ohmic resistor. When

$|V_{ds}| > |V_g| - |V_t|$ and the device is on, the device is in the saturation regime, where the relationship between V_{ds} and I_d becomes non-linear [1], [3], [8].
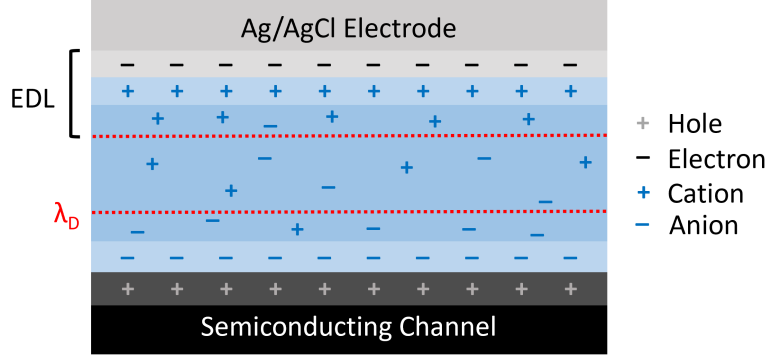
Liquid-Gating and Debye Length

Figure 1.2.: A diagram of the formation of an electric double layer (EDL) under an applied voltage between source and liquid-gate electrodes, with a *p*-type semiconductor used for the channel thin-film. Electric double layers are present at both the gate-electrolyte interface and semiconductor-electrolyte interface. Adapted from [3], [11], [12].

Understanding the ionic behaviour of the gate electrolyte used in a liquid-gated device setup gives insight into the gating and sensing behaviour of the setup. When a voltage is applied at the liquid-gate, the charged ions in solution move to form two electric double layers, one at the interface between the electrolyte and gate electrode, and one at the interface between electrolyte and semiconducting channel, as shown in Figure 1.2. The gate capacitance is a series combination of the capacitance of each EDL in series with quantum capacitance C_Q [3], [13]. The Gouy-Chapman-Stern model splits the EDL into two distinct regions, the first being a compact layer of ions, the Stern layer, and the second being a more diffuse layer, the Gouy-Chapman layer [12]. The surface potential of the solid-electrolyte interface exponentially decreases across the diffuse region of the double-layer; the characteristic length of this potential screening is known as Debye length, λ_D. The typical electrolyte Debye length is on a nanometer scale, therefore the bulk electrolyte acts as an insulator, similar to the silicon dioxide dielectric in the back-gated configuration. The Stern layer capacitance is inversely proportional to the Debye length, and therefore decreased λ_D corresponds to increased gate capacitance [3], [4], [11], [13].

$$\lambda_D = \sqrt{\frac{\epsilon_0 \epsilon_r k_b T}{2 N_A q^2 I}} \tag{1.1}$$

The equation for Debye length λ_D in an electrolyte solution is given by Equation 1.1, where ϵ_0 is vacuum permittivity, ϵ_r is the relative permittivity of the electrolyte, B is the Boltzmann constant, T is absolute temperature in K, N_A is the Avogadro number, q is the elementary charge and I is ionic strength in mmol L^{-1}. When temperature is kept constant, λ_D only depends on the ionic strength of the electrolyte and not on any attributes of the gate electrode or channel. Successive dilutions of a particular electrolyte will increase the Debye length: for 1× PBS, λ_D is 0.7 nm, for 0.1× PBS, λ_D is 2.3 nm, for 0.01× PBS λ_D is 7.3 nm and so on. This means gate capacitance is directly dependent on the electrolyte used and its concentration. A 1× PBS electrolyte gives a gate capacitance several orders of magnitude larger than that of a silicon oxide backgate. A larger capacitance significantly increases the effect of electrostatic gating on the channel current, often described as increased electrostatic coupling between gate and channel. A liquid-gated device with low Debye length will therefore be highly sensitive to electrostatic changes across a small voltage range [3], [4], [11], [13], [14].

However, a decreased Debye length also has disadvantages for sensing. Electrostatic potentials outside of the electrolyte-channel electrical double layer are effectively screened from the channel. Electrical double layers will also form around charged receptors within the solution. The combined screening effect means signals due to potential changes in charged biomolecules within the bulk electrolyte will have no effect on gating of the channel, and therefore no effect on I_d. Interactions between the analyte and any receptor element must therefore occur within the Debye length, and so a tradeoff exists between channel sensitivity and the size of the sensitive region above the channel. Many medium or large proteins will require a relatively dilute electrolyte for analyte capture to be detected by the channel, which may not reflect the intended environment for biosensor application [3], [15], [16]. Other approaches to increasing Debye length without reducing device sensitivity have therefore also been trialled. One approach involves attaching a layer of polyethylene glycol polymer (PEG) to the channel, limiting the approach of counterions. This increases Debye length at the electrolyte-channel interface while preserving the capacitance of the electrolyte-gate interface, keeping device sensitivity relatively high [17]–[19].

1.2.2. Electrical Characterisation

Both carbon nanotube field effect transistors and graphene field-effect transistors are naturally ambipolar. Applying a gate voltage V_g to the gate of an ambipolar thin-film transistor influences the amount and type of available charge carriers for conduction [2], [7], [9]. The current-voltage plots for a given transistor are known as the 'characteristic curves' of the transistor. The plot of I_d against V_g at constant V_{ds} is known as the 'transfer' characteristic curve at that source-drain voltage, while the I-V curve of I_d against V_{ds} at constant V_g is known as the 'source-drain' or 'output' characteristic curve at that gate voltage [1], [3]. The transfer characteristics are governed by the gate capacitance, as discussed in Section 1.2.1. Both back-gated and liquid-gated transfer

characteristics from ambipolar thin-film transistors are shown in Figure 1.3. Taking regular transfer measurements of a graphene or carbon nanotube device is not only useful in building a complete picture of device behaviour, but also may help to ensure devices are kept highly sensitive to electrostatic gating effects through redistributing charge in the channel [20].

A variety of quantitative parameters can be extracted from the transfer characteristics of a thin-film transistor. A quantitative summary of a range of TFT parameters can be found in the thin-film transistor study by Petti *et al.* [1]. The parameters of particular interest here are transconductance, on-off ratio, threshold voltage and subthreshold swing. Transconductance and on-off ratio are discussed below, while threshold voltage and subthreshold swing are discussed for the carbon nanotube network case specifically in Section 1.4.3. Other behaviours observed when measuring currents present in a thin-film device are also discussed below, including source-gate leakage current and the hysteresis and real-time signal drift of source-drain current.

Transconductance

In the linear regime, transconductance at a specific gate voltage is given by $g_m = |dI_d/dV_g|$. Transconductance indicates how responsive the device is to electrostatic gating at a given gate voltage. In other words, when g_m is large, small changes in V_g can significantly modulate channel current I_d, which is useful for sensing [9], [11]. Transconductance at a given gate voltage is also proportional to the mobility (movement) of charge carriers in the device channel, and therefore depends on the scattering properties of the material [1], [8], [21]. The transconductance at a specific gate voltage can be found from performing a linear fit in a small region around that voltage on the transfer curve. Linear fits for transconductance at $V_g = 0$ V are shown for a back-gated device in Figure 1.3 (a), and a liquid-gated device in Figure 1.3 (b), which give values of $g_m = 0.05$ μS and $g_m = 1$ μS respectively. The difference of several orders of magnitude between back-gated and liquid-gated transconductance corresponds to the difference of several orders of magnitude between back and liquid-gated gate capacitance [2], [3]. Improved transconductance is therefore a significant advantage of the use of the liquid-gate.

On-off Ratio

Another important attribute of the transfer characteristic curve for all thin-film FETs is the on-off current ratio. On-off current ratio is the ratio of the current through a device when gated fully 'off' with a positive voltage, I_{off}, to the current through the device when gated fully 'on' with a negative voltage, I_{on}. The off current in an ambipolar FET can be defined as the minimum current during the transfer sweep, where the majority carrier transitions from being holes to electrons or *vice versa* [1], [22]. For example, for the channel shown in Figure 1.3 (b), $I_{on} = 741.5$ nA and $I_{off} = 0.2$ nA. Therefore, the on-off ratio I_{on}/I_{off} is ~ 3000. In contrast, even when 10 V is applied, the backgated

Figure 1.3.: Examples of field-effect transistor transfer characteristics taken at $V_{ds} = 100$ mV from two different device channels. A linear scale is used in (a) and (b), while a logarithmic scale is used in (c) and (d). The curves in (a) and (c) are from backgated channels, while the curves in (b) and (d) are from liquid-gated channels. The linear fit with gradient corresponding to transconductance at $V_g = 0$ V is shown in (a) and (b) with a dotted red line. The "on" current in (c) and (d) is shown with a red horizontal line, while the "off" current in (d) is shown with a blue horizontal line.

device shown in Figure 1.3 (a) is never gated fully off. Being able to traverse both on and off regimes over a limited voltage interval is another advantage of the liquid-gated configuration. Having a low off current is desirable as it corresponds to low power consumption by the transistor [21]. Overall, on-off ratio of a device is a useful figure of merit for switching which is relatively simple to both find and present.

Gate Leakage

Application of higher voltages to the gate in both the liquid-gate and back-gate cases can result in significant leakage currents through the gate. These currents mean that the insulating layer at the gate producing the capacitive effect no longer acts as an insulator, adversely affecting transistor behaviour and contributing to sensor drift that may be mistaken for signal responses to analyte[3], [19], [20]. In the case of back-gated devices, gate leakage occurs due to conduction through the oxide dielectric. If the gate voltage produces an electric field exceeding the dielectric strength of the oxide, dielectric breakdown can occur, where the oxide layer no longer acts as an insulator. Breakdown results from voltage-induced oxygen vacancies in the SiO_2 lattice forming a conductive path through the insulator [23]. In the liquid-gated case, the choice of electrolyte determines the appropriate voltage range for electrical characterisation, since excessive voltages will drive electrolysis and induce redox reactions. For water-based electrolytes, gate voltages must be kept within the $\pm$ 1 V range [3], [11], [14]. In normal operation, gate current should appear negligible on a linear scale for both the back-gated and liquid-gated cases, as shown in Figure 1.4.

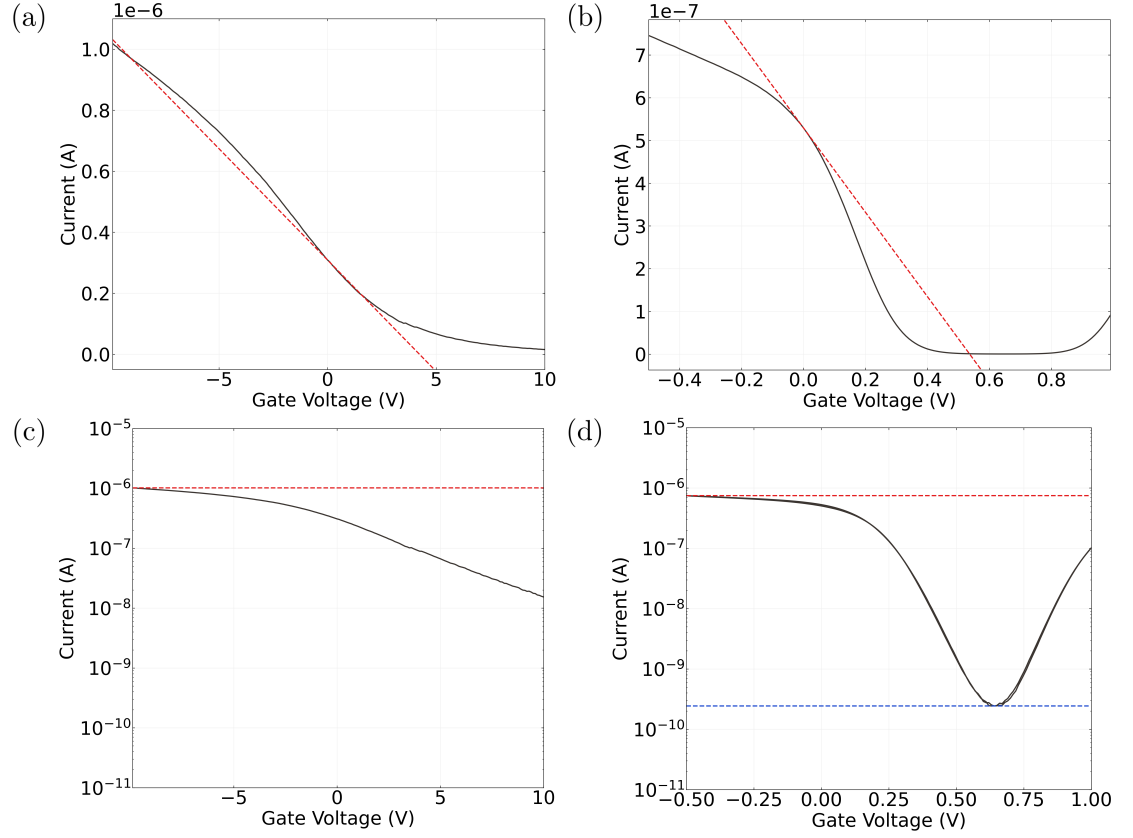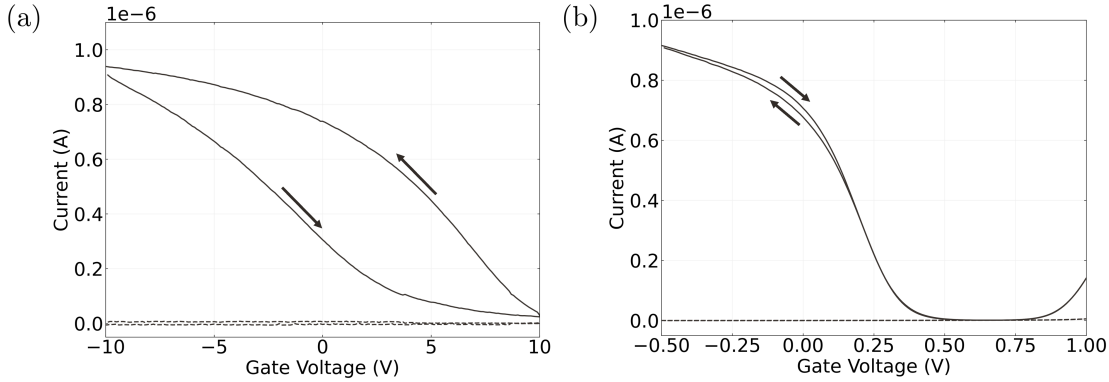Figure 1.4.: Field-effect transistor transfer characteristics taken at $V_{ds} = 100$ mV from two different device channels on a linear scale. Forward and reverse sweeps are shown for the back-gated case (a) and the liquid-gated case (b), with the direction of each sweep indicated by an arrow. A sweep rate of $V_{ds} = 100$ mV/sample was used for the back-gated device and a sweep rate of $V_{ds} = 10$ mV/sample was used for the liquid-gate device. The gate current measured during each sweep is also shown with a dotted line.

Hysteresis and Baseline Drift

Thin-film transistor devices typically exhibit some degree of hysteresis, where the history of channel current affects future current behaviour. Hysteresis in carbon nanotube and graphene field-effect transistors is a result of filling or emptying of slow-discharge charge traps in the channel environment. These charge traps effectively dope the silicon dioxide insulator or the insulator-channel interface, which results from gate bias stress or dopant adsorption [14], [24]–[26]. A capacitive gating effect from charged ions also contributes to hysteresis, from the use of a electrolyte-gated environment or from charged surface contamination [4], [14]. Due to hysteresis, sweeping V_g forwards across a set voltage range will result in a different I_d-V_g characteristic curve than subsequently sweeping over V_g in the reverse direction. Hysteresis depends on the voltage range used for characterisation, the sweep rate and the environment of the transistor channel [14], [25]. Hysteresis in both the back-gated and liquid-gated cases are shown in Figure 1.4. Hysteresis is significantly lower for the liquid-gated case, which may be due to the reduced voltage range and sweep rate used. However, this change may also result from a reduction in trap states in the silicon dioxide layer due to the use of a liquid-gate.

Memory effects are also present during current measurement when both source-drain and source-gate voltages are kept constant. These changes appear as a slow change in current, and are referred to here as either signal drift or baseline drift. In more extreme cases, baseline drift can obscure or even be confused with current changes attributable to analyte interaction during real-time sensing. Signal drift occurs both in ambient conditions and in a vacuum environment, and cannot be accounted for by changes in room temperature and ambient lighting alone. While research into signal drift is ongoing, it appears to be a hysteretic effect resulting from changes in trap states over time [20], [26], [27]. The high demand for characterisation equipment in a standard device laboratory means that waiting over three hours for baseline drift to settle is impractical, and furthermore, extended periods of voltage application may degrade bio-functionalised devices [20]. Since trap states are unavoidable to a degree [28], [29], data analysis that accounts for baseline drift was therefore explored in some detail in this thesis.

1.3. Graphene Field-Effect Transistors

1.3.1. Graphene Properties

Graphene is a 2-dimensional material which consists of covalently bonded carbon atoms in a dense lattice of hexagonal cells [2], [24], [30], [31]. Graphene can be used to create a variety of low-dimensional graphitic nanomaterials, including carbon nanotubes [24] (see Section 1.4.1). Monolayer and bilayer graphene are zero band-gap semiconductors, where traversing the electronic bandstructure in different directions gives rise to either

metallic or semiconducting behaviour [24]. Adding more graphene layers adds more complexity to the bandstructure, with significant overlap between bands and reduced carrier mobility. When 10 or more layers are present, the structure behaves as 3D graphite [11], [31]. First isolated in 2004 [30], monolayer graphene has many desirable electronic properties. Charge carrier transport is ballistic over submicrometer distances at room temperature, and as graphene is metallic even at the Dirac point, this transport is not inhibited by a Schottky barrier at the metal contacts of a device [30], [31]. Graphene is also a highly chemically stable material. In particular, it will not readily oxidise in an electrolyte solution due to having a large 'electrochemical window'; in other words, it is too chemically stable to take part in electrochemical reactions within a large range of applied voltages [2], [11].
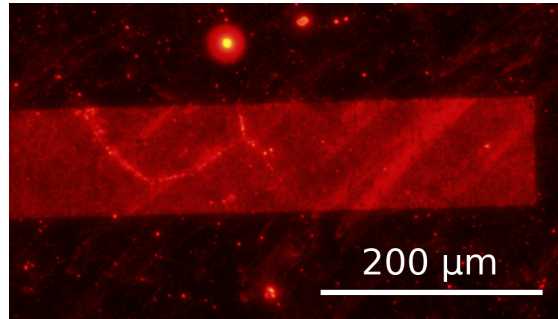
Graphene Folds

Figure 1.5.: Fluorescence image of a strip of graphene on silicon dioxide surface functionalised with Rhodamine B dye. Bright lines are visible on the left side of the graphene surface which correspond to preferential attachment of dye along the graphene folds.

Graphene folding (also referred to as warping or wrinkling) on the scale of tens of nanometers occurs at many locations on a graphene monolayer. These folds primarily result from the chemical vapour deposition process onto copper used in the creation of graphene films. The thermal contraction of copper exceeds that of graphene during the rapid cooling that takes place after deposition. Since the graphene is pinned to the surface, this leads to slight folding of the monolayer. Transferring graphene from the rough copper to a relatively smooth Si/SiO$_2$ wafer may also contribute to wrinkling [32]–[34]. Folds may be up to ~ 6 nanometers in height [33]. These folds help to mechanically stabilise the graphene layer, but have significant negative effects on charge transport [31], [33], [34]. Folds also exhibit enhanced reactivity due to their low radius of curvature [32]. This is demonstrated in Figure 1.5, where the fluorescent Rhodamine B dye preferentially bonds to folded regions, leading to particularly dense functionalisation in these regions. This behaviour has been previously observed for the decoration of graphene with pentacene molecules [34]. Other defects influencing surface reactivity

include grain boundaries and point defects in the crystal structure [32], [34].

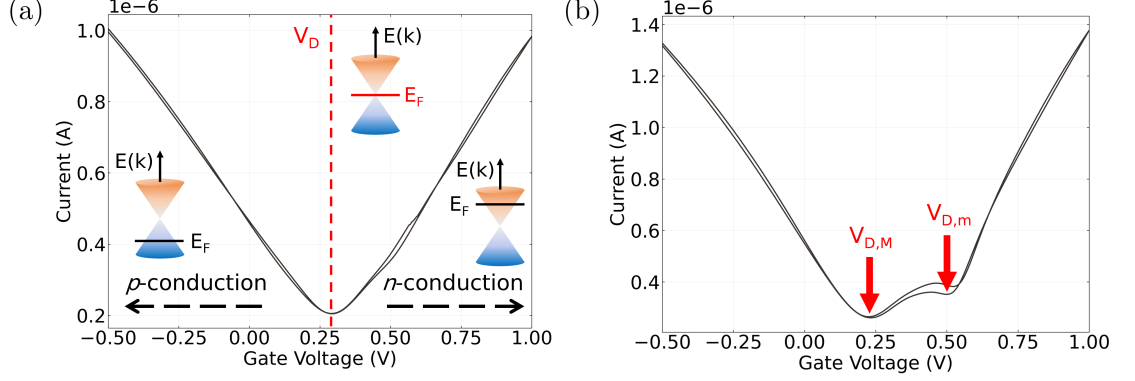### 1.3.2. Electrical Characterisation

Figure 1.6.: Liquid-gated transfer characteristics of two graphene field-effect transistor channels. In (a), the Dirac point voltage is indicated by a red dotted line, and regions of hole conduction and electron conduction are also shown. The relative Fermi energy in each region is shown on graphene bandstructure insets (adapted from [11], [31]). The graphene channel in (b) has double conduction minima, which are highlighted with red arrows.

When a gate voltage V_g is applied to the channel of a graphene device, the Fermi energy of the graphene is shifted and surface charge density is altered [11], [13], [30]. An increase in available charge means an increase in carriers available for conduction and increased I_d [31].

The transfer sweep behaviour is that of an ambipolar semiconductor, except there is no characteristic 'off' regime. The minimum conductance obtainable by gating occurs at what is known as the neutrality or Dirac point, where the population of charge carriers is at a minimum [11], [30]. At voltages close to the Dirac voltage, a mixed state exists where both electrons and holes are present. As gate voltage moves left away from the Dirac voltage, holes begin to dominate conduction, while when gate voltage is moved to the right of the Dirac voltage, electrons dominate [30].

As gate voltage is increased or decreased away from the Dirac voltage, conductivity increases linearly [30]. Typically, a monolayer graphene channel will conduct holes at zero gate voltage, which is due to the presence of atmospheric dopants such as water. By removing these dopants, the Dirac point feature can be brought closer to the zero gate voltage position on the transfer curve, indicating graphene is naturally a mixed-carrier conductor [30].

The on-off ratio of the graphene transfer curve shown is 5. As graphene lacks a bandgap, there is a minimum possible conductance for graphene devices, which leads to a rela-

tively small on-off ratio [30], [31]. This attribute is a drawback of the graphene FET in sensing applications when compared with carbon nanotube transistors [30]. However, the transconductance of the curve at $V_g = 0$ V, $g_m = 1$ µS, is similar to the liquid-gated transconductance of a carbon nanotube device shown earlier. The on-off ratio may be decreased by the presence of significant graphene folding due to diffusive transport of carriers along the folds [33].

while the Dirac voltage is 0.29 V.

Quantative measurement of leftward shift in transfer curve

I compared the transfer characteristics after then rinse steps to the pristine characteristics Transfer shifts where current drops to zero are excluded (indicates delamination/damage to channel)

1.3.3. Sensing Behaviour

The large surface-to-volume ratio of graphene makes it highly sensitive to intermolecular interactions and therefore appropriate for use in sensing applications [2], [11]. An analyte molecule can be detected using a graphene channel by observing the change in current that occurs when a charged analyte alters the channel Fermi level [11], [13].

Sensing may be dominated by interactions occurring at the graphene folds [32].

1.4. Random-Network Carbon Nanotube Field-Effect Transistors

1.4.1. Carbon Nanotube Properties

Since their initial identification in 1991 [35], a wide range of applications for carbon nanotubes (CNTs) have been proposed, due to their small mass, elasticity, strength, and unique electronic properties. A single-walled carbon nanotube (SWCNT) consists of a monolayer graphene sheet rolled up into a cylinder, while a multi-walled carbon nanotube (MWCNT) consists of several monolayer graphene cylinders where smaller cylinders are coaxially contained by larger cylinders [3], [6], [7], [21], [36]. Multi-walled carbon nanotubes can suffer from significant scattering at defects leading to diffusive electron motion [36]. However, single-walled carbon nanotubes are relatively defect-free, and carrier transport within nanotubes is near-ballistic at room temperature, resulting in high carrier mobility [3], [6], [7], [21], [36]. The momentum of charge carriers in a single-walled carbon nanotube is quantised, confining carriers to 2-dimensional slices across the 3-dimensional graphene bandstructure. If a slice contains a bandgap, the carbon nanotube behaves as a semiconductor (s-CNT); if not, the nanotube behaves as a metal (m-CNT) [24]. The high surface-to-volume ratio of small-diameter single-walled

carbon nanotubes makes them extremely sensitive and therefore particularly suitable for sensing applications [3], [4], [6]. Like graphene, carbon nanotubes have a large potential window, and can be used safely in a liquid-gate environment without undergoing redox reactions [11].
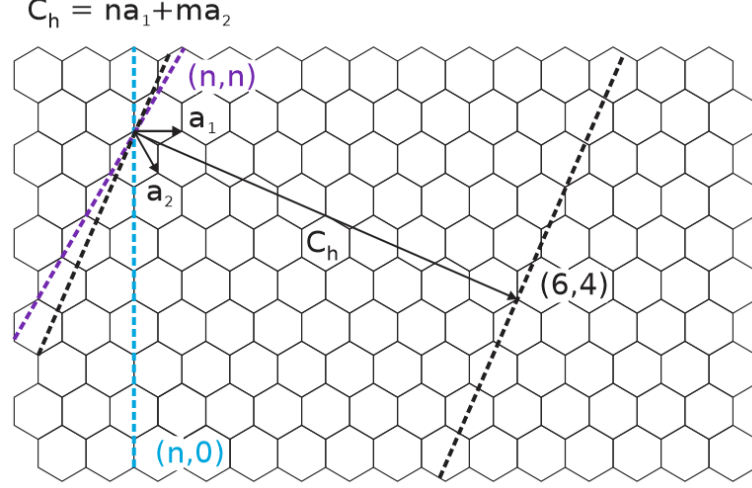

Figure 1.7.: Diagram illustrating how a graphene sheet can be rolled up at various angles to form carbon nanotubes. The two black dotted lines represent boundaries which can be cut across and then brought into contact to form a cylinder. The cylinder here is referred to by the integer pair (6,4), as the chiral vector C_h, the vector perpendicular to the cut through the sheet, is given by $C_h = 6a_1 + 4a_2$. The chiral vector forms the circumference of the rolled carbon nanotube. The left edge in the zigzag $(n,0)$ and armchair (n,n) cases are shown with a blue and purple dotted line respectively. The location of the right edge (diameter of the nanotube) is determined by the value chosen for n. Adapted from [36], [37].

The chirality and diameter of a carbon nanotube determines its electronic bandstructure and whether it has semiconducting or metallic characteristics [3], [7], [8], [24], [36], [38]. The chirality indices of a nanotube (n,m) determines the chiral angle at which hexagons wind around the nanotube relative to the longitudinal axis of the nanotube. This chiral angle is the angle between the chiral vector $\mathbf{C_h} = n\mathbf{a_1} + m\mathbf{a_2}$, which maps to the circumference of the nanotube, and the basis vector $\mathbf{a_1}$, which is parallel to a row of hexagons. The size of the chiral angle θ is given by Equation 1.2, the diameter of the resulting carbon nanotube is given by $d = |C_h|/\pi$ [37].

$$\theta = \arcsin \frac{\sqrt{3}m}{2\sqrt{n^2 + nm + m^2}}, n > m \qquad (1.2)$$

When $m = 0$, $\theta = 0°$, and the resulting carbon nanotube has a 'zigzag' structure; when

$m = n$, $\theta = 30°$, and the carbon nanotube has an 'armchair' structure. When θ is between $0° - 30°$, the structure is referred to as 'chiral' [36], [37]. When $n - m = 3z$, where z is an integer, the resulting carbon nanotube is metallic $-$ for example, if $n = 5$ and $m = 5$, $z = 0$, therefore the tube is metallic. All other nanotubes are semiconducting, including the (6,4) chiral nanotube described in Figure 1.7. Out of the chiral arrangements available, two-thirds of the possible structures are semiconducting while one-third is metallic [36].

1.4.2. Carbon Nanotube Networks

Although a single carbon nanotube can be used as the channel of a thin-film transistor, this approach has significant drawbacks. An alternative approach is to use a large-scale network of carbon nanotubes as the transistor channel. Here, the individual electrical properties of the CNTs are averaged out across the network, which minimises device-to-device variation. Furthermore, the large area of coverage both ensures high currents and increases the likelihood of interactions with the local environment in sensing applications [6], [8], [39], [40]. Carbon nanotube networks can either be aligned or randomly deposited [3], [6]; in this thesis, randomly deposited networks were fabricated using facile solution-deposition methods. Important attributes of a carbon nanotube film include the density of the network (number of nanotubes per unit area), the ratio of metallic to semiconducting nanotubes present, and the distribution of nanotube diameters present [3], [6]. The strong van der Waals forces between carbon nanotubes lead to them bundling together within a network. These bundles may contain many nanotubes of different size and chirality [6], [39]–[41].

In a network carbon nanotube device with metal electrodes, transistor switching is primarily governed by band bending at the interfaces between each electrode and the semiconducting carbon nanotubes. The difference in Fermi level between each material leads to a a flow of charge across each interface until the Fermi levels equilibrate and a Schottky barrier forms. These barriers are effectively electric dipole layers whose net electric fields restrict the further flow of charge at each interface. This band bending process depends on the work function of the metal, so the type of metal determines the type of charge being restricted. For example, a high work function metal bends the valence band of the semiconductor towards the Fermi level of the metal, creating a low barrier for holes but a high barrier for electrons at each interface [7], [26]. Channel current results primarily from quantum tunnelling through these Schottky barriers. The Schottky barriers at the metal electrodes result in one type of charge dominating flow, referred to as unipolar behaviour. However, if the barrier size is low for both holes and electrons, they can flow simultaneously through the channel, referred to as ambipolar behaviour [7], [42].

The behaviour of carbon nanotube network transistors is also influenced by a variety of potential barriers existing at junctions between carbon nanotubes. A prominent example

is the Schottky barriers existing at junctions between metallic and semiconducting nanotubes (m-s junctions) [40], [41], [43]. These potential barriers cause increased resistance at these junctions relative to other points in the network [41], [44]. When the channel length is much larger than that of individual nanotubes, channel current must pass through junctions placed along percolation pathways. If only one pathway exists across a sparse network, the network density is at the 'percolation threshold'. If a network is below the percolation threshold, the channel cannot conduct [39], [43], [44]. When a network with density well above percolation contains a low proportion of semiconducting nanotubes, percolating pathways which only contain metallic nanotubes exist. A device with this film will be highly conductive but cannot be gated [41], [43]. Fixing the density but increasing the proportion of s-CNTs means m-s junctions become more prevalent. The introduced Schottky barriers cause a dramatic drop in conductance. As the proportion of s-CNTs approaches 100%, semiconducting pathways with no metallic junctions emerge, and conductance sharply increases once more [43].

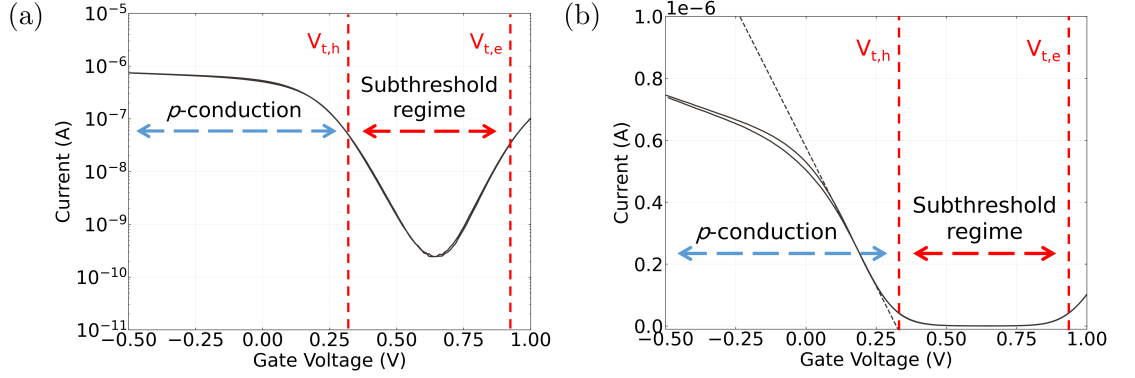### 1.4.3. Electrical Characterisation

Figure 1.8.: Liquid-gated transfer characteristics of a single carbon nanotube network field-effect transistor channel, using a logarithmic scale in (a) and using a linear scale in (b) to emphasise different features of the same dataset. The subthreshold slope is shown with a black dotted line, while the threshold voltages are shown with red dotted lines. The ON and OFF regimes are also indicated on both figures. $V_{ds} = 100$ mV was placed across the channel.

Like graphene transistors, mixed-chirality carbon nanotube transistors are naturally ambipolar: they can conduct both electrons and holes. An applied gate voltage V_g alters the Fermi energy of the semiconducting nanotubes, changing the size of the Schottky barriers present, and therefore changing the amount and type of charge flowing through the channel [7], [42], [45]. I_d mainly consists of holes at highly negative gate voltages, and mainly consists of electrons at highly positive voltages. At intermediary voltages, both electrons and holes flow [4], [7]. Transistor behaviour can be made unipolar through doping the semiconducting carbon nanotubes or by choosing an electrode metal with a

particularly high work function, increasing the Schottky barrier for one type of charge [4], [6], [7]. For example, the use of gold electrodes promotes *p*-type behaviour over *n*-type behaviour due to the work function of the metal; ambient adsorption of oxygen will weakly dope the semiconducting carbon nanotubes and likewise promote *p*-type behaviour [3], [6], [24].

A variety of parameters can be extracted which reflect the morphology of the carbon nanotube network. Partial alignment of a random-network carbon nanotube network maximises the transconductance of a device, as this creates more semiconducting pathways, increasing current while preserving the presence of gateable junctions within the network [6], [8], [10], [21], [44]. The on-off ratio of a carbon nanotube device is largely decided by the ratio of s-CNTs to m-CNTs. The relative proportion of metallic carbon nanotubes in the network determines the size of I_{off}. Therefore, unlike a graphene device, the off current can be readily reduced by eliminating percolating metallic pathways for increased I_{on}/I_{off} [6], [10], [21], [39]. In a liquid-gated environment, the gate leakage current of a sparse carbon nanotube transistor can approach I_d, leading to significant device noise. A dense network or a graphene device can therefore give enhanced signal-to-noise ratio during sensing [11]. Noyce *et al.* found that fully-on back-gated carbon nanotube devices typically exhibit a ~ 3 hour period of steep signal drift, followed by steady-state current flow. This settling behaviour was both reversible and highly characteristic of a particular channel, and could be modelled using a sum of three exponentials [20].

Threshold Voltage

The threshold voltage V_t of a unipolar transistor is equal to the gate voltage required to prevent the flow of charge carriers across the channel, often referred to as turning the device off [1], [3]. In ambipolar devices, two separate threshold voltages exist for each type of charge carrier, $V_{t,h}$ and $V_{t,e}$, which are shown in Figure 1.8 on both a linear (a) and logarithmic (b) scale. In the region between these gate voltages, known as the subthreshold regime, both holes and electrons flow through the channel [7], [46]. If percolating pathways consisting entirely of m-CNTs are present, I_{off} flows through these pathways, as conduction through metallic nanotubes is largely unaffected by changes in V_g [41], [43]. If there are no unblocked m-CNT pathways, I_{off} is entirely due to Schottky barrier tunnelling [7]. V_t can be estimated by extrapolating the trendline of the linear region of the transfer characteristics to the V_g axis. The intercept is approximately equal to the threshold voltage when V_{ds} is close to zero, as shown in Figure 1.8 (b) [1], [8], [47]. This is only a rough estimate of the actual device V_t, but is sufficient when comparing the gating behaviour of different devices [8].
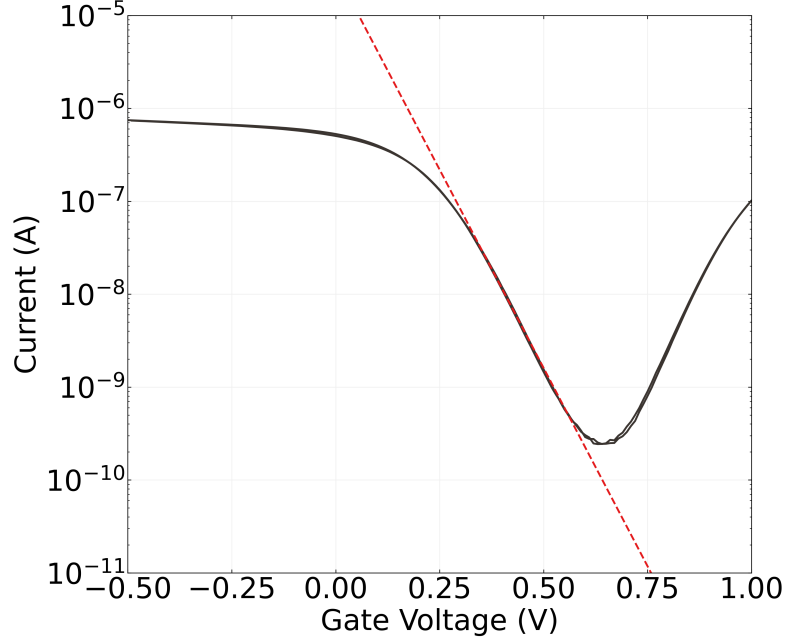
Figure 1.9.: A carbon nanotube network transfer sweep with $V_{ds} = 100$ mV on a logarithmic scale. Threshold voltage is shown with a black dotted line, while subthreshold slope is shown with a red dotted line.

Subthreshold Slope

The subthreshold slope S is a measure of how rapidly a transistor approaches the minimum current I_{off}. The subthreshold slope is often referred to using its reciprocal value, the subthreshold swing, which is equivalent to the change in V_g required to change I_d by one order of magnitude. This figure of merit is strongly related to the gate capacitance of the device. As the slope exponentially approaches the off current in the subthreshold regime, it can be fitted with a linear trendline on a logarithimic scale. [1], [47]. A linear trendline fitted to the logarithm of the subthreshold regime is shown in Figure 1.9, where the gradient corresponds to subthreshold slope. A high subthreshold slope (greater than 0.01 decades/mV) reduces power consumption and required operating voltage of the sensor device [1]. Some studies have found that sensor devices showed better signal-to-noise ratio when gated in the subthreshold regime, where small voltage changes in response to analyte can cause exponential current changes along the subthreshold slope [48], [49].

1.4.4. Sensing

As all atoms are at the surface of the carbon nanotube structure, nanotubes are very sensitive to their surroundings and therefore suitable for sensing use [3], [4], [6]. The chirality and diameter of a carbon nanotube affects both its coupling with the gate and

its surface chemistry, which determines the sensing mechanisms available to a single CNT. Only s-CNTs can be electrostatically gated; m-CNTs, bent nanotubes and larger diameter nanotubes are typically more reactive [6], [8], [32], [34]; and the nanotube chirality (n, m) can determine the strength of binding to DNA in a base sequence-dependent manner [10]. Carbon nanotubes have been used for vapour-phase sensing since 2000, when Kong *et al.* found that the resistance over a single CNT channel was modified when exposed to gas molecules like NO_2 and NH_3 [50]. In a range of gas sensor applications, carbon nanotubes can detect the presence of analyte down to the parts per billion level [4], [51]. However, in general, device specificity of response is low, where nanotubes respond to many different analytes in a similar manner. To enhance specificity, surface functionalisation is often performed using either inorganic or biological materials, such as enzymes, antibodies, aptamers and proteins [3], [4], [6].

For carbon nanotube network transistors, sensing mechanisms include electrostatic gating, charge transfer, Schottky barrier modulation, capacitance modulation and charge scattering. Response mechanisms may take place at the gate, the junctions between channel and contact, or at the semiconductor channel [2], [8], [42], [52], [53]. Modification of the channel-metal Schottky barrier can dominate sensing activity, and this can complicate the identification of mechanisms underlying the sensing behaviour [6], [53], [54]. The encapsulation layer shown in Figure 1.1 is added to separate the electrodes from the channel-metal junction and prevent these responses [3], [42]. If there are few Schottky barriers present in the network of an encapsulated device, the predominant sensing mechanism is either charge transfer from the analyte to channel [52], [55] or electrostatic gating [42]. The charge transfer mechanism involves direct addition of charge carriers to the channel, while the gating mechanism results from a nearby charge inducing an opposite polarity charge in the channel. Both changes alter the relationship between V_g and I_d and shift the carrier threshold voltages [2], [3], [8]. However, when Schottky and other potential barriers are frequent, barrier modulation may make a significant contribution to sensing responses, especially at densities close to the percolation threshold [40], [53].

1.5. Summary

A. Vapour System Hardware

Table A.1.: Major components used in construction of the vapour delivery system described in this thesis.

Description	Part No.	Manufacturer
Mass flow controller, 20 sccm full scale	GE50A013201SBV020	MKS Instruments
Mass flow controller, 200 sccm full scale	GE50A013202SBV020	MKS Instruments
Mass flow controller, 500 sccm full scale	FC-2901V	Tylan
Analogue flowmeter, 240 sccm max. flow	116261-30	Dwyer
Micro diaphragm pump	P200-B3C5V-35000	Xavitech
Analogue flow controller, for micro diaphragm pump	X3000450	Xavitech
10 mL Schott bottle	218010802	Duran
PTFE connection cap system	Z742273	Duran
Baseline VOC-TRAQ flow cell, red	043-951	Mocon
Humidity and temperature sensor	T9602	Telaire
Enclosure, for humidity and temperature sensor	MC001189	Multicomp Pro

B. Python Code for Data Analysis

B.1. Code Repository

The code used for general analysis of field-effect transistor devices in this thesis was written with Python 3.8.8. Contributors to the code used include Erica Cassie, Erica Happe, Marissa Dierkes and Leo Browning. The code is located on GitHub and the research group OneDrive, and is available on request.

B.2. Atomic Force Microscope Histogram Analysis

The purpose of this code is to analyse atomic force microscope (AFM) images of carbon nanotube networks in .xyz format taken using an atomic force microscope and processed in Gwyddion (see **?@sec-afm-characterisation**). It was originally designed by Erica Happe in Matlab, and adapted by Marissa Dierkes and myself for use in Python. The code imports the .xyz data and sorts it into bins 0.15 nm in size for processing. To perform skew-normal distribution fits, both *scipy.optimize.curve_fit* and *scipy.stats.skewnorm* modules are used in this code.

B.3. Raman Spectroscopy Analysis

The purpose of this code is to analyse a series of Raman spectra taken at different points on a single film (see **?@sec-raman-characterisation**). Data is imported in a series of tab-delimited text files, with the low wavenumber spectrum ($100 \text{ cm}^{-1} - 650 \text{ cm}^{-1}$) and high wavenumber spectrum ($1300 \text{ cm}^{-1} - 1650 \text{ cm}^{-1}$) imported in separate datafiles for each scan location.

B.4. Field-Effect Transistor Analysis

The purpose of this code is to analyse electrical measurements taken of field-effect transistor (FET) devices. Electrical measurements were either taken from the Keysight 4156C Semiconductor Parameter Analyser, National Instruments NI-PXIe or Keysight B1500A Semiconductor Device Analyser as discussed in **?@sec-electrical-characterisation**;

the code is able to analyse data in .csv format taken from all three measurement setups. The main Python file in the code base consists of three related but independent modules: the first analyses and plots sensing data from the FET devices, the second analyses and plots transfer characteristics from channels across a device, and the third compares individual channel characteristics before and after a modification or after each of several modifications. The code base also features a separate config file and style sheet which govern the behaviour of the main code. The code base was designed collaboratively by myself and Erica Cassie over GitHub using the Sourcetree Git GUI.

Bibliography

[1] Luisa Petti, Niko Münzenrieder, Christian Vogt, et al. "Metal oxide semiconductor thin-film transistors for flexible electronics". In: *Applied Physics Reviews* 3.2 (June 2016), p. 21303. ISSN: 19319401. DOI: 10.1063/1.4953034. URL: /aip/apr/article/3/2/021303/123579/Metal-oxide-semiconductor-thin-film-transistors.

[2] Thien Toan Tran and Ashok Mulchandani. "Carbon nanotubes and graphene nano field-effect transistor-based biosensors". In: *TrAC Trends in Analytical Chemistry* 79 (May 2016), pp. 222–232. ISSN: 0165-9936. DOI: 10.1016/J.TRAC.2015.12.002.

[3] Bajramshahe Shkodra, Mattia Petrelli, Martina Aurora Costa Angeli, et al. "Electrolyte-gated carbon nanotube field-effect transistor-based biosensors: Principles and applications". In: *Applied Physics Reviews* 8.4 (Dec. 2021), p. 41325. ISSN: 19319401. DOI: 10.1063/5.0058591. URL: /aip/apr/article/8/4/041325/1076095/Electrolyte-gated-carbon-nanotube-field-effect.

[4] Xuesong Yao, Yalei Zhang, Wanlin Jin, et al. "Carbon Nanotube Field-Effect Transistor-Based Chemical and Biological Sensors". In: *Sensors 2021, Vol. 21, Page 995* 21.3 (Feb. 2021), p. 995. ISSN: 1424-8220. DOI: 10.3390/S21030995. URL: https://www.mdpi.com/1424-8220/21/3/995/htm%20https://www.mdpi.com/1424-8220/21/3/995.

[5] Paul K. Weimer. "The TFT—A New Thin-Film Transistor". In: *Proceedings of the IRE* 50.6 (1962), pp. 1462–1469. ISSN: 00968390. DOI: 10.1109/JRPROC.1962.288190.

[6] Qing Cao and John A. Rogers. "Ultrathin Films of Single-Walled Carbon Nanotubes for Electronics and Sensors: A Review of Fundamental and Applied Aspects". In: *Advanced Materials* 21.1 (Jan. 2009), pp. 29–53. ISSN: 1521-4095. DOI: 10.1002/ADMA.200801995. URL: https://onlinelibrary.wiley.com/doi/full/10.1002/adma.200801995%20https://onlinelibrary.wiley.com/doi/abs/10.1002/adma.200801995%20https://onlinelibrary.wiley.com/doi/10.1002/adma.200801995.

[7] Phaedon Avouris. "Electronics with carbon nanotubes". In: *Physics World* 20.3 (Mar. 2007), p. 40. ISSN: 2058-7058. DOI: 10.1088/2058-7058/20/3/32. URL: https://iopscience.iop.org/article/10.1088/2058-7058/20/3/32%20https://iopscience.iop.org/article/10.1088/2058-7058/20/3/32/meta.

[8]   Zhongyu Li, Mengmeng Xiao, Chuanhong Jin, et al. "Toward the Commercialization of Carbon Nanotube Field Effect Transistor Biosensors". In: *Biosensors 2023, Vol. 13, Page 326* 13.3 (Feb. 2023), p. 326. ISSN: 2079-6374. DOI: 10.3390/ BIOS13030326. URL: https://www.mdpi.com/2079-6374/13/3/326/htm% 20https://www.mdpi.com/2079-6374/13/3/326.

[9]   I. Heller, S. Chatoor, J. Männik, et al. "Comparing the weak and strong gate-coupling regimes for nanotube and graphene transistors". In: *physica status solidi (RRL) – Rapid Research Letters* 3.6 (Sept. 2009), pp. 190–192. ISSN: 1862-6270. DOI: 10.1002/PSSR.200903157. URL: https://onlinelibrary.wiley.com/doi/full/ 10.1002/pssr.200903157%20https://onlinelibrary.wiley.com/doi/abs/10.1002/ pssr.200903157%20https://onlinelibrary.wiley.com/doi/10.1002/pssr.200903157.

[10]   Nima Rouhi, Dheeraj Jain, and Peter John Burke. "High-performance semiconducting nanotube inks: Progress and prospects". In: *ACS Nano* 5.11 (Nov. 2011), pp. 8471–8487. ISSN: 19360851. DOI: 10.1021/NN201828Y. URL: https://pubs. acs.org/doi/full/10.1021/nn201828y.

[11]   Yasuhide Ohno, Kenzo Maehashi, and Kazuhiko Matsumoto. "Graphene biosensor". In: *Frontiers of Graphene and Carbon Nanotubes: Devices and Applications* (Jan. 2015), pp. 91–104. DOI: 10.1007/978-4-431-55372-4_7/FIGURES/13. URL: https://link.springer.com/chapter/10.1007/978-4-431-55372-4_7.

[12]   Pranjala Tiwari and Dawid Janas. "Emergent pseudocapacitive behavior of single-walled carbon nanotube hybrids: a materials perspective". In: *Materials Chemistry Frontiers* 6.17 (Aug. 2022), pp. 2386–2412. ISSN: 20521537. DOI: 10.1039/ D2QM00146B. URL: https://pubs.rsc.org/en/content/articlehtml/2022/qm/ d2qm00146b%20https://pubs.rsc.org/en/content/articlelanding/2022/qm/ d2qm00146b.

[13]   Iddo Heller, Sohail Chatoor, Jaan Männik, et al. "Influence of electrolyte composition on liquid-gated carbon nanotube and graphene transistors". In: *Journal of the American Chemical Society* 132.48 (Dec. 2010), pp. 17149–17156. ISSN: 00027863. DOI: 10.1021/JA104850N. URL: https://pubs.acs.org/doi/full/10. 1021/ja104850n.

[14]   Haomin Wang, Yihong Wu, Chunxiao Cong, et al. "Hysteresis of electronic transport in graphene transistors". In: *ACS Nano* 4.12 (Dec. 2010), pp. 7221–7228. ISSN: 19360851. DOI: 10.1021/NN101950N/SUPPL_FILE/NN101950N_SI_001.PDF. URL: https://pubs.acs.org/doi/full/10.1021/nn101950n.

[15]   Eric Stern, Robin Wagner, Fred J. Sigworth, et al. "Importance of the debye screening length on nanowire field effect transistor sensors". In: *Nano Letters* 7.11 (Nov. 2007), pp. 3405–3409. ISSN: 15306984. DOI: 10.1021/NL071792Z/SUPPL_FILE/ NL071792ZSI20070910_015801.PDF. URL: https://pubs.acs.org/doi/full/10. 1021/nl071792z.

[16] Esteban Piccinini, Sebastián Alberti, Gabriel S. Longo, et al. "Pushing the Boundaries of Interfacial Sensitivity in Graphene FET Sensors: Polyelectrolyte Multilayers Strongly Increase the Debye Screening Length". In: *Journal of Physical Chemistry C* 122.18 (May 2018), pp. 10181–10188. ISSN: 19327455. DOI: 10.1021/ACS.JPCC.7B11128/ASSET/IMAGES/MEDIUM/JP-2017-11128H_M007.GIF. URL: https://pubs.acs.org/doi/full/10.1021/acs.jpcc.7b11128.

[17] Ning Gao, Teng Gao, Xiao Yang, et al. "Specific detection of biomolecules in physiological solutions using graphene transistor biosensors". In: *Proceedings of the National Academy of Sciences of the United States of America* 113.51 (Dec. 2016), pp. 14633–14638. ISSN: 10916490. DOI: 10.1073/PNAS.1625010114/SUPPL_FILE/PNAS.201625010SI.PDF. URL: https://www.pnas.org/doi/abs/10.1073/pnas.1625010114.

[18] Vladimir Kesler, Boris Murmann, and H. Tom Soh. "Going beyond the Debye Length: Overcoming Charge Screening Limitations in Next-Generation Bioelectronic Sensors". In: *ACS Nano* 14.12 (Dec. 2020), p. 16194. ISSN: 1936086X. DOI: 10.1021/ACSNANO.0C08622. arXiv: 2007.13201. URL: /pmc/articles/PMC7761593/%20/pmc/articles/PMC7761593/?report=abstract%20https://www.ncbi.nlm.nih.gov/pmc/articles/PMC7761593/.

[19] Faris M. Albarghouthi, Nicholas X. Williams, James L. Doherty, et al. "Passivation Strategies for Enhancing Solution-Gated Carbon Nanotube Field-Effect Transistor Biosensing Performance and Stability in Ionic Solutions". In: *ACS Applied Nano Materials* 5.10 (Oct. 2022), pp. 15865–15874. ISSN: 25740970. DOI: 10.1021/ACSANM.2C04098. URL: https://doi.org/10.1021/acsanm.2c04098.

[20] Steven G. Noyce, James L. Doherty, Zhihui Cheng, et al. "Electronic Stability of Carbon Nanotube Transistors under Long-Term Bias Stress". In: *Nano Letters* 19.3 (Mar. 2019), pp. 1460–1466. ISSN: 15306992. DOI: 10.1021/ACS.NANOLETT.8B03986. URL: https://pubs.acs.org/doi/full/10.1021/acs.nanolett.8b03986.

[21] Nima Rouhi, Dheeraj Jain, and Peter John Burke. "Nanoscale devices for large-scale applications". In: *IEEE Microwave Magazine* 11.7 (Dec. 2010), pp. 72–80. ISSN: 15273342. DOI: 10.1109/MMM.2010.938569.

[22] H. Y. Zheng and N. O.V. Plank. "Facile fabrication of carbon nanotube network thin film transistors for device platforms". In: *International Journal of Nanotechnology* 14.1-6 (2017), pp. 505–518. ISSN: 14757435. DOI: 10.1504/IJNT.2017.082473.

[23] A. Padovani, D. Z. Gao, A. L. Shluger, et al. "A microscopic mechanism of dielectric breakdown in SiO2 films: An insight from multi-scale modeling". In: *Journal of Applied Physics* 121.15 (Apr. 2017), p. 155101. ISSN: 10897550. DOI: 10.1063/1.4979915/1007563. URL: /aip/jap/article/121/15/155101/1007563/A-microscopic-mechanism-of-dielectric-breakdown-in.

[24] Paul L. McEuen, Michael S. Fuhrer, and Hongkun Park. "Single-walled carbon nanotube electronics". In: *IEEE Transactions on Nanotechnology* 1.1 (2002), pp. 78–84. ISSN: 1536125X. DOI: 10.1109/TNANO.2002.1005429.

[25] Woong Kim, Ali Javey, Ophir Vermesh, et al. "Hysteresis Caused by Water Molecules in Carbon Nanotube Field-Effect Transistors". In: *NANO LETTERS* 3.2 (2003), pp. 193–198. DOI: 10.1021/nl0259232.

[26] Y. Bargaoui, M. Troudi, P. Bondavalli, et al. "Gate bias stress effect in single-walled carbon nanotubes field-effect-transistors". In: *Diamond and Related Materials* 84 (Apr. 2018), pp. 62–65. ISSN: 0925-9635. DOI: 10.1016/J.DIAMOND.2018.03.011.

[27] H. Lin and S. Tiwari. "Localized charge trapping due to adsorption in nanotube field-effect transistor and its field-mediated transport". In: *Applied Physics Letters* 89.7 (Aug. 2006), p. 73507. ISSN: 00036951. DOI: 10.1063/1.2337104. URL: /aip/apl/article/89/7/073507/332595/Localized-charge-trapping-due-to-adsorption-in.

[28] D. J. DiMaria, E. Cartier, and D. Arnold. "Impact ionization, trap creation, degradation, and breakdown in silicon dioxide films on silicon". In: *JAP* 73.7 (1993), pp. 3367–3384. ISSN: 0021-8979. DOI: 10.1063/1.352936. URL: https://ui.adsabs.harvard.edu/abs/1993JAP....73.3367D/abstract.

[29] Philip G. Collins, M. S. Fuhrer, and A. Zettl. "1/f noise in carbon nanotubes". In: *Applied Physics Letters* 76.7 (Feb. 2000), pp. 894–896. ISSN: 0003-6951. DOI: 10.1063/1.125621. URL: /aip/apl/article/76/7/894/112362/1-f-noise-in-carbon-nanotubes.

[30] K. S. Novoselov, A. K. Geim, S. V. Morozov, et al. "Electric field in atomically thin carbon films". In: *Science* 306.5696 (Oct. 2004), pp. 666–669. ISSN: 00368075. DOI: 10.1126/SCIENCE.1102896.

[31] A. K. Geim and K. S. Novoselov. "The rise of graphene". In: *Nature Materials 2007 6:3* 6.3 (Mar. 2007), pp. 183–191. ISSN: 1476-4660. DOI: 10.1038/nmat1849. URL: https://www.nature.com/articles/nmat1849.

[32] Shichao Zhao, Sumedh P. Surwade, Zhiting Li, et al. "Photochemical oxidation of CVD-grown single layer graphene". In: *Nanotechnology* 23.35 (Aug. 2012), p. 355703. ISSN: 0957-4484. DOI: 10.1088/0957-4484/23/35/355703. URL: https://iopscience.iop.org/article/10.1088/0957-4484/23/35/355703%20https://iopscience.iop.org/article/10.1088/0957-4484/23/35/355703/meta.

[33] Wenjuan Zhu, Tony Low, Vasili Perebeinos, et al. "Structure and electronic transport in graphene wrinkles". In: *Nano Letters* 12.7 (July 2012), pp. 3431–3436. ISSN: 15306984. DOI: 10.1021/NL300563H/SUPPL_FILE/NL300563H_SI_001.PDF. URL: https://pubs.acs.org/doi/full/10.1021/nl300563h.

[34] Manisha Chhikara, Egon Pavlica, and Gvido Bratina. "Grafold-driven nucleation of pentacene on graphene". In: *Surface Science* 609 (Mar. 2013), pp. L5–L8. ISSN: 0039-6028. DOI: 10.1016/J.SUSC.2012.11.001.

[35] Sumio Iijima. "Helical microtubules of graphitic carbon". In: *Nature 1991 354:6348* 354.6348 (1991), pp. 56–58. ISSN: 1476-4687. DOI: 10.1038/354056a0. URL: https://www.nature.com/articles/354056a0.

[36] Cees Dekker. "Carbon Nanotubes as Molecular Quantum Wires". In: *Physics Today* 52.5 (May 1999), pp. 22–28. ISSN: 0031-9228. DOI: 10.1063/1.882658. URL: /physicstoday / article / 52 / 5 / 22 / 410816 / Carbon - Nanotubes - as - Molecular - Quantum-WiresThe.

[37] Xiaoxing Lu and Zhong Hu. "Mechanical property evaluation of single-walled carbon nanotubes by finite element modeling". In: *Composites Part B: Engineering* 43.4 (June 2012), pp. 1902–1913. ISSN: 13598368. DOI: 10.1016 / J.COMPOSITESB.2012.02.002. URL: https://www.researchgate.net / publication / 257545663 _ Mechanical _ property _ evaluation _ of _ single - walled_carbon_nanotubes_by_finite_element_modeling.

[38] R. Martel, T. Schmidt, H. R. Shea, et al. "Single- and multi-wall carbon nanotube field-effect transistors". In: *Applied Physics Letters* 73.17 (Oct. 1998), pp. 2447–2449. ISSN: 0003-6951. DOI: 10.1063/1.122477. URL: /aip/apl/article/73/17/2447/1023171/Single-and-multi-wall-carbon-nanotube-field-effect.

[39] L. Hu, D. S. Hecht, and G. Gruner. "Percolation in transparent and conducting carbon nanotube networks". In: *Nano Letters* 4.12 (Dec. 2004), pp. 2513–2517. ISSN: 15306984. DOI: 10.1021/NL048435Y. URL: https://pubs.acs.org/doi/full/10.1021/nl048435y.

[40] Thanihaichelvan Murugathas, Leo A. Browning, Marissa P. Dierkes, et al. "Metallic-semiconducting junctions create sensing hot-spots in carbon nanotube FET aptasensors near percolation". In: *Biosensors and Bioelectronics* 130 (Apr. 2019), pp. 408–413. ISSN: 0956-5663. DOI: 10.1016/J.BIOS.2018.09.021.

[41] M. S. Fuhrer, J. Nygård, L. Shih, et al. "Crossed nanotube junctions". In: *Science (New York, N.Y.)* 288.5465 (Apr. 2000), pp. 494–497. ISSN: 1095-9203. DOI: 10.1126 / SCIENCE.288.5465.494. URL: https://pubmed.ncbi.nlm.nih.gov/10775104/.

[42] Iddo Heller, Anne M. Janssens, Jaan Männik, et al. "Identifying the mechanism of biosensing with carbon nanotube transistors". In: *Nano Letters* 8.2 (Feb. 2008), pp. 591–595. ISSN: 15306984. DOI: 10.1021/NL072996I. URL: https://pubs.acs.org/doi/full/10.1021/nl072996i.

[43] Mark A. Topinka, Michael W. Rowell, David Goldhaber-Gordon, et al. "Charge transport in interpenetrating networks of semiconducting and metallic carbon nanotubes". In: *Nano Letters* 9.5 (May 2009), pp. 1866–1871. ISSN: 15306984. DOI: 10.1021/NL803849. URL: https://pubs.acs.org/doi/full/10.1021/nl803849e.

[44] Ho Kyun Jang, Jun Eon Jin, Jun Hee Choi, et al. "Electrical percolation thresholds of semiconducting single-walled carbon nanotube networks in field-effect transistors". In: *Physical Chemistry Chemical Physics* 17.10 (Feb. 2015), pp. 6874–6880. ISSN: 1463-9084. DOI: 10.1039/C4CP05964F. URL: https://pubs.rsc.org/en/content/articlehtml/2015/cp/c4cp05964f%20https://pubs.rsc.org/en/content/articlelanding/2015/cp/c4cp05964f.

[45] Takeshi Nakanishi, Adrian Bachtold, and Cees Dekker. "Transport through the interface between a semiconducting carbon nanotube and a metal electrode". In: *Physical Review B* 66.7 (Aug. 2002), p. 073307. ISSN: 01631829. DOI: 10.1103/PhysRevB.66.073307. URL: https://journals.aps.org/prb/abstract/10.1103/PhysRevB.66.073307.

[46] Ciril Reiner-Rozman, Melanie Larisika, Christoph Nowak, et al. "Graphene-Based Liquid-Gated Field Effect Transistor for Biosensing: Theory and Experiments". In: *Biosensors & bioelectronics* 70 (Aug. 2015), p. 21. ISSN: 18734235. DOI: 10.1016/J.BIOS.2015.03.013. URL: /pmc/articles/PMC4707551/%20pmc/articles/PMC4707551/?report=abstract%20https://www.ncbi.nlm.nih.gov/pmc/articles/PMC4707551/.

[47] S.M. Sze and Kwok K. Ng. "Physics of Semiconductor Devices". In: *Physics of Semiconductor Devices* (Oct. 2006). DOI: 10.1002/0470068329. URL: https://onlinelibrary.wiley.com/doi/book/10.1002/0470068329.

[48] Iddo Heller, Jaan Mãnnik, Serge G. Lemay, et al. "Optimizing the signal-to-noise ratio for biosensing with carbon nanotube transistors". In: *Nano Letters* 9.1 (Jan. 2009), pp. 377–382. ISSN: 15306984. DOI: 10.1021/NL8031636. URL: https://pubs.acs.org/doi/full/10.1021/nl8031636.

[49] Xuan P A Gao, Gengfeng Zheng, and Charles M Lieber. "Subthreshold Regime has the Optimal Sensitivity for Nanowire FET Biosensors". In: (2010). DOI: 10.1021/nl9034219. URL: https://pubs.acs.org/sharingguidelines.

[50] Jing Kong, Nathan R. Franklin, Chongwu Zhou, et al. "Nanotube molecular wires as chemical sensors". In: *Science (New York, N.Y.)* 287.5453 (Jan. 2000), pp. 622–625. ISSN: 1095-9203. DOI: 10.1126/SCIENCE.287.5453.622. URL: https://pubmed.ncbi.nlm.nih.gov/10649989/.

[51] Jialuo Chen, Ardalan Lotfi, Peter J. Hesketh, et al. "Carbon nanotube thin-film-transistors for gas identification". In: *Sensors and Actuators B: Chemical* 281 (Feb. 2019), pp. 1080–1087. ISSN: 0925-4005. DOI: 10.1016/J.SNB.2018.10.035.

[52] Yann Battie, Olivier Ducloux, Philippe Thobois, et al. "Gas sensors based on thick films of semi-conducting single walled carbon nanotubes". In: *Carbon* 49.11 (Sept. 2011), pp. 3544–3552. ISSN: 0008-6223. DOI: 10.1016/J.CARBON.2011.04.054.

[53] Anthony Boyd, Isha Dube, Georgy Fedorov, et al. "Gas sensing mechanism of carbon nanotubes: From single tubes to high-density networks". In: *Carbon* 69 (Apr. 2014), pp. 417–423. ISSN: 0008-6223. DOI: 10.1016/J.CARBON.2013.12.044.

[54] Vera Schroeder, Suchol Savagatrup, Maggie He, et al. "Carbon Nanotube Chemical Sensors". In: *Chemical reviews* 119.1 (Jan. 2019), pp. 599–663. ISSN: 1520-6890. DOI: 10.1021/ACS.CHEMREV.8B00340. URL: https://pubmed.ncbi.nlm.nih.gov/30226055/.

[55] Brett Lee Allen, Padmakar D. Kichambare, and Alexander Star. "Carbon Nanotube Field-Effect-Transistor-Based Biosensors". In: *Advanced Materials* 19.11 (June 2007), pp. 1439–1451. ISSN: 1521-4095. DOI: 10.1002/ADMA.200602043. URL: https://onlinelibrary.wiley.com/doi/full/10.1002/adma.200602043%20https://onlinelibrary.wiley.com/doi/abs/10.1002/adma.200602043%20https://onlinelibrary.wiley.com/doi/10.1002/adma.200602043.